Journal of Food Engineering 349 (2023) 111434

Contents lists available at ScienceDirect

Journal of Food Engineering

journal homepage: www.elsevier.com/locate/jfoodeng

Development and validation of analytical charts for microwave assisted thermal pasteurization of selected food products

Yonas Gezahegn [a], Yoon-Ki Hong [a], Juming Tang [a,*], Patrick Pedrow [b], Shyam S. Sablani [a], Fang Liu [a], Zhongwei Tang [a]

[a] Department of Biological Systems Engineering, Washington State University, P.O Box 646120, Pullman, WA, 99164-6120, USA
[b] School of Electrical Engineering & Computer Science, Washington State University, P.O Box 642752, Pullman, WA, 99164-2752, USA

ARTICLE INFO

Keywords:
Analytical chart
Dielectric properties
Heating rate
Microwave heating
Pasteurization
Preheating temperature

ABSTRACT

For process development using an industrial Microwave Assisted Thermal Pasteurization System (MAPS), it is desirable to have effective tools that allow accurate prediction of heating rates in pre-packaged foods. This research aimed to develop engineering charts that illustrate the relationships among the dielectric properties of foods, preheating temperature, product thickness, and heating rate in the microwave heating section of MAPS. We selected three different foods, namely mashed potatoes, peas, and rice, in this study. Three complementary G-T (Gezahegn-Tang) charts were developed using MATLAB software by applying Maxwell's and heat transfer equations with measured physical properties of the selected foods. Experiments were conducted with mashed potato samples using a pilot-scale MAPS unit to validate the charts. The temperature profiles measured at the cold spots of the food samples in the microwave heating section of MAPS were positively correlated with predicted temperatures from the chart ($R^2 > 0.96$); more than 95% of the standardized residuals were in the range of −2 to 2 °C. The charts are able to estimate microwave heating rate at the cold spots in food packages based on food dielectric properties and package thickness. They can also be used to help select an optimal preheating temperature for the maximum heating rate. This research demonstrated the possibility of using validated G-T charts to assist food companies in developing pasteurization schedules based on MAPS for the commercial production of different packaged ready-to-eat (RTE) meals.

1. Introduction

Over the past 50 years, the food industry and related research communities have invested enormous resources and efforts in exploring microwave heating as an alternative to conventional surface heating methods in traditional thermal processing operations for pre-packaged foods (Chandrasekaran et al., 2013; Tang, 2015). In the USA, a 915 MHz single-mode Microwave Assisted Thermal Pasteurization System (MAPS) has been developed at Washington State University for pasteurization of chilled RTE meals (Tang et al., 2018). Several recent studies have demonstrated the expected high quality and long shelf life of RTE meals produced by MAPS in comparison with traditional thermal processing and novel high pressure pasteurization (Inanoglu et al., 2021; Montero et al., 2020; Qu et al., 2021).

The MAPS consists of four main sections, for preheating, heating, holding and cooling, respectively (Fig. 1). In operation, pre-packaged foods are immersed in circulating water and transported via a conveyor through the four sections. In the preheating section, the food reaches an initial equilibrium temperature before being moved through the heating section where the food is heated to a pasteurization temperature (70–90 °C) at the cold spot in food packages. The selection of the specific pasteurization temperature depends on the desired shelf-life in refrigeration (Peng et al., 2017). The circulating water at a pre-set temperature in the microwave heating section helps reduce edge heating of the packaged foods and improve heating uniformity (Tang, 2015). Following microwave heating, the food is held for a certain period in the holding section to reach the target lethality and then moved to a cooling section to reach a room temperature of 23 °C (Fig. 1) (Tang et al., 2018).

Several factors influence the heating rates in foods during processing in MAPS. Those factors include dielectric properties, specific heat, salt content, thickness of foods, as well as preheating temperature and applied microwave power. It is, therefore, difficult to accurately predict the microwave heating rate in a food package. For validation of new thermal processes for pathogen control, including microwave heating,

* Corresponding author.
E-mail addresses: yonas.gezahegn@wsu.edu (Y. Gezahegn), jtang@wsu.edu (J. Tang).

https://doi.org/10.1016/j.jfoodeng.2023.111434
Received 15 September 2022; Received in revised form 13 January 2023; Accepted 27 January 2023
Available online 3 February 2023

the United States Food and Drug Administration (FDA) requires a study of the heat penetration with temperature measurement at the determined cold spot under the worst-case heating conditions (FDA, 2016; IFTPS, 2014). The ability to quantify the influence of the above factors on heating rates at the cold spot in food packages would benefit food companies in developing safe process schedules for MAPS systems (Jain et al., 2019).

The relative dielectric permittivity (ε_r^*) of food is a critical factor that influences microwave heating. This property is defined as a complex number in the following equation (Nelson, 1973; Ryynänen, 1995):

$$\varepsilon_r^* = \varepsilon'_r - j\varepsilon''_r \quad (1)$$

where $j = \sqrt{-1}$, ε'_r is the relative dielectric constant (the ability of food to store electric energy), and ε''_r is the relative dielectric loss factor (the ability of food to convert microwave energy to thermal energy). The subscript "*r*" indicates the dielectric properties are relative to free space. The relative dielectric constant and loss factor are often referred to dielectric constant (ε') and loss factor (ε''), respectively, without the subscript "*r*." The dielectric properties are affected by food composition, mainly moisture and salt contents, temperature, and frequency. Water contributes to the dipole effect, and dissolved salts contribute to the ionic conduction effect of the loss factor (İcier and Baysal, 2004; Ryynänen, 1995; Tang, 2015).

The food thickness is another key factor that influences microwave penetration to the food package central layer in MAPS. As discussed by Jain et al. (2019), when 1×10^3 V/m incident electric field was applied with 0° phase difference between the microwave waves to the top and bottom sides of a 15 mm thick sample ($\varepsilon' = 40$ and $\varepsilon'' = 30$), the power dissipation of 1.7×10^6 W/m^3 was attained at the center layer of the sample in a 915 MHz single-mode cavity. While keeping all other conditions the same, increasing the thickness to 30 mm reduced the power dissipation by 44% to 0.95×10^6 W/m^3.

In our earlier studies, three-dimensional computer simulations that coupled Maxwell's with heat transfer equations were used to predict temperature increases in moving food packages in Microwave Assisted Thermal Sterilization (MATS) processes (Chen et al., 2008; Jain et al., 2018; Resurreccion et al., 2013). MATS system uses the same microwave heating cavity design as MAPS (Tang, 2015; Tang et al., 2018). These studies required high-performance computing power, yet the simulation results did not provide clear quantitative relationships among different factors that directly influence heating rates at the cold spot in the packaged foods in microwave systems. To address this drawback, Jain et al. (2019) developed a simple analytic equation to predict the electric field distribution along the depth of a rectangular food in MATS processing. After determining the electric field, the prospective power dissipation and heating rate at the center layer can be calculated. The equations for those calculations are included in Section 3.1.

The complex relationships among the food physical properties and processing conditions make it difficult for food companies to directly use the analytical equation to predict product temperature under different processing conditions. Hence, Hong et al. (2021) developed an engineering chart based on this equation to estimate the microwave heating rate in packaged foods in MAPS. The considered variables include food thickness, food dielectric loss factor, and thermal properties. But the ranges of the dielectric property values of the foods considered in the chart development were very narrow. In addition, the chart is limited to only one constant dielectric constant value, namely $\varepsilon' = 70$. The influence of temperature on dielectric property change was not considered.

Therefore, this research aimed to: i) develop a more comprehensive set of analytical charts that quantify the relationships among the food dielectric properties, packaged food thickness, and microwave power dissipation for predicting the center layer heating rate of a packaged food processed in the MAPS, ii) validate the chart with a pilot-scale MAPS using mashed potato samples with different dielectric properties and packaging thicknesses, and iii) illustrate the use of the charts for prediction of the microwave heating rate in MAPS and selection of the optimal preheating temperature for the maximum heating rate.

2. Materials and methods

2.1. Mathematical models

A single-mode microwave heating cavity of MAPS (Fig. 1) is illustrated in Fig. 2. The simplified mathematical models for heating rate prediction for food in the microwave cavity were developed under the following assumptions.

i. 915 MHz electromagnetic plane waves in TE_{10} mode entered the horn applicators from both the top and bottom sides with a 0° phase difference (i.e., the two entering waves are synchronized with no phase difference). The waves traveled perpendicularly through the circulating water to the food.
ii. The food samples were solid, homogeneous, isotropic, and packed in a rectangular-shaped container; the polymer package material had a negligible dielectric loss factor.
iii. The microwave power was considered the only heat source, and the convective and conductive heating from the circulating water at the pasteurization temperature to the center layer of the packaged food was considered negligible for short microwave heating time (typically in 2–4 min).

Using the above conditions and assumptions, Jain et al. (2019) developed the following equation to calculate electric field intensity (E) in V/m inside the food as a function of distance Z along the thickness of the package:

$$E = \frac{T_{w/f} E_0}{1 + R_{w/f} e^{-\gamma_f L}} \left(e^{-\gamma_f Z} + e^{-\gamma_f (L-Z)} \right) \quad (2)$$

where, subscript w and f represent the circulating water and food sample, respectively; E_0, T, R, γ, L and Z represent the average incident electric field intensity at food surfaces (the interfaces between water and food), the microwave transmission coefficient, reflection coefficient,

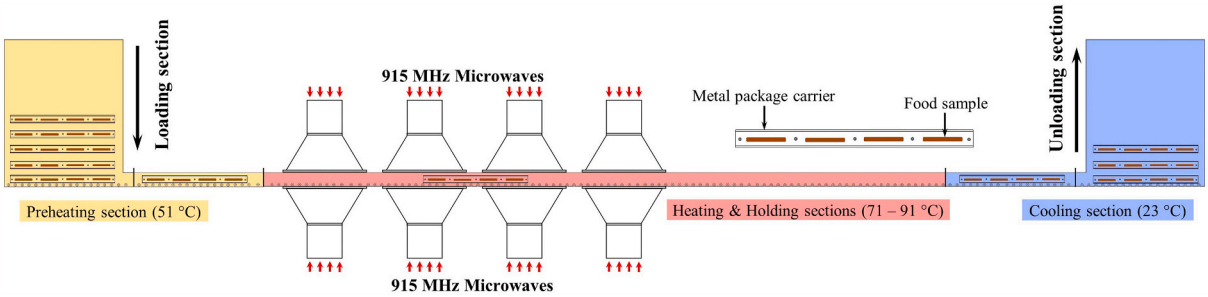

Fig. 1. Schematic design of Microwave Assisted Thermal Pasteurization System (MAPS).

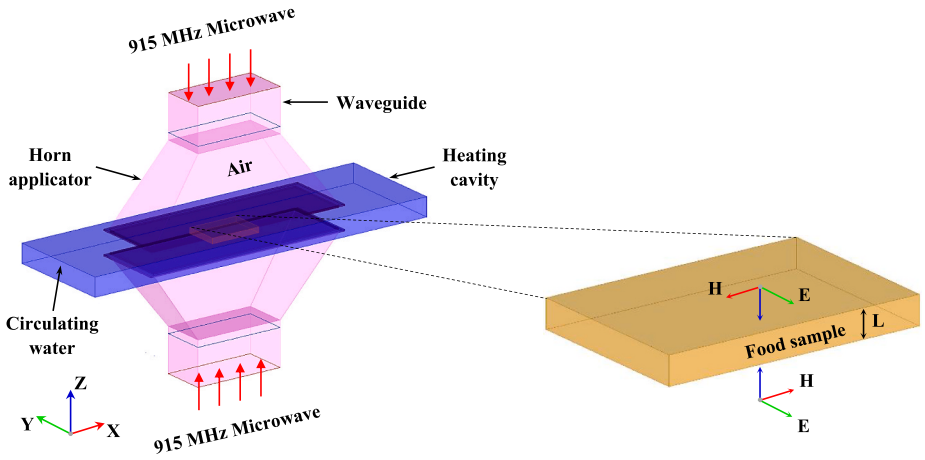

Fig. 2. A single-mode microwave heating cavity with a food sample, L = thickness.

and propagation constant, the thickness of food, and the distance from the water and food interface, respectively. The average incident electric field (E_0) in the MAPS was determined with preliminary experiments through reverse calculation (using Eqs. (13) and (2)) from the measured temperature and heating rate profile in mashed potato samples. For food samples less than 30 mm thick, the average $E_0 = 0.5 \times 10^3$ V/m; for 30–40 mm thick, $E_0 = 0.4 \times 10^3$ V/m. Previous research by Hong et al. (2021) also reported a similar E_0 (0.527×10^3 V/m) for a 22 mm thick food sample.

The propagation constant (γ) is expressed as:

$$\gamma = \alpha + j\beta \tag{3}$$

where the real part, α (Np/m), is the attenuation constant; the imaginary part, β (rad/m), is the phase constant. Both constants can be calculated from:

$$\alpha = \frac{2\pi f}{c}\sqrt{\frac{\varepsilon'}{2}\left(\sqrt{1+\left(\frac{\varepsilon''}{\varepsilon'}\right)^2}-1\right)} \tag{4}$$

$$\beta = \frac{2\pi f}{c}\sqrt{\frac{\varepsilon'}{2}\left(\sqrt{1+\left(\frac{\varepsilon''}{\varepsilon'}\right)^2}+1\right)} \tag{5}$$

where f and c are the frequency and speed of light (3×10^8 m/s), respectively (Balanis, 2012). In a lossy medium, the transmission ($T_{w/f}$) and reflection ($R_{w/f}$) coefficients are quantified as:

$$T_{w/f} = \frac{2\eta_f}{\eta_w + \eta_f} \tag{6}$$

$$R_{w/f} = \frac{\eta_f - \eta_w}{\eta_w + \eta_f} \tag{7}$$

where η_f and η_w represent the complex intrinsic impedance of the food sample and circulating water, respectively. The intrinsic impedances are expressed as:

$$\eta_f = \frac{\eta_o}{\sqrt{\varepsilon_f^*}} \tag{8}$$

$$\eta_w = \frac{\eta_o}{\sqrt{\varepsilon_w^*}} \tag{9}$$

where η_o is the intrinsic impedance of free space (377Ω), ε_f^* is the electric permittivity of food, and ε_w^* is the electric permittivity of the circulating water (Balanis, 2012).

Eqs. (10) and (11) define the microwave power dissipation, P (W/m^3) and heating rate, dT/dt (°C/sec) within the food, respectively, all of which vary with distance (Z) (Balanis, 2012; Jain et al., 2019):

$$P(z) = 2\pi f \varepsilon_0 \varepsilon'' |E|^2 \tag{10}$$

$$\frac{dT}{dt} = \frac{P(Z)}{\rho C_P} \tag{11}$$

where ε_0 is the dielectric permittivity of vacuum (8.85×10^{-12} F/m), ρCp (J/°C.m^3) is the volumetric specific heat of the food.

2.2. Experimental validation

2.2.1. Sample preparations and property measurements

Dielectric and thermal properties of mashed potatoes, peas and rice were used to develop the analytical charts. The three samples were chosen to represent three different food categories, namely, vegetables (mashed potatoes), legumes (peas), and cereals (rice). The food samples were prepared with various salt contents (Food grade, Morton, Chicago, IL, USA) to alter the dielectric properties. Mashed potato samples were prepared by first mixing 0.75% (wt/wt) low acyl gellan gum (Modernist Pantry LLC., Eliot, ME, USA) in warm distilled water. When the temperature reached 90 °C, 3% (wt/wt) potato flakes (Oregon Potato Company, Pasco, WA, USA) and 0.15% (wt/wt) calcium chloride (Macron Fine Chemicals, Randor, PA, USA) were added gradually while mixing. Divalent cations from dissolved calcium chloride would facilitate the gelation of the food samples upon cooling (Tang et al., 1994, 1997). The solution was then cooled to 70–80 °C, then salt (Morton salt Inc., Chicago, IL, USA) and 0.4% (wt/wt) titanium dioxide (Lorann oils Inc., Lansing, MI, USA) were added. The titanium dioxide was used to create an opaque white color to dictate the heating pattern easily. As the temperature went down to 55–65 °C, 2% (wt/wt) fructose and 1% (wt/wt) lysine were added as a precursor of the M-1 chemical marker; then the sample was poured into rectangular trays (Silgan, Union, MO, USA). The added salt contents were 0, 0.1, 0.6, 1, 1.5, and 2% (wt/wt). The above formulae and sample preparation procedure were developed by Bornhorst et al. (2017) to study heating uniformity in MAPS based on color changes due to Maillard reactions. For pea preparation, dried white peas (Swad, Skokie, IL, USA) were soaked overnight at room temperature and were boiled in distilled water with a pea-to-water ratio of 1:1.5 (wt/wt) at 95 °C for 60 min. Then salt was added, and the peas were ground before being filled into the trays. The added salt contents were 0, 0.1, 0.2, 0.5, 1 and 2% (wt/wt). For rice, medium-size grains (Nishiki, Los Angeles, CA, USA) were cooked in distilled water with a rice-to-water ratio of 1:1.2 (wt/wt) at 95 °C for 40 min with different added salt contents of 0, 0.2, 0.5, 1, 1.5 and 2% (wt/wt). The above procedures were developed by Jain et al. (2019).

The dielectric properties (ε' & ε") of mashed potatoes, peas, and rice samples were measured at 915 MHz from 20 to 120 °C using an HP 8752C Network Analyzer and an 85070 B open-end coaxial dielectric probe (Agilent Technologies, Santa Clara, CA, USA) following the procedures described in Gezahegn et al. (2021). The sample was heated in a tightly sealed custom-built sample cell to perform measurements at higher temperatures. A detailed description of the test cell is provided in Gezahegn et al. (2021). The dielectric properties of the circulating water (reverse osmosis purified) used in MAPS were also measured at 91 °C. The loss factor (ε") of the circulating water was 3, and the dielectric constant (ε') was 60. The measurements were made in triplicates. A differential scanning calorimeter (DSC, Q1000, TA Instruments, New Castle, DE, USA) was used to measure the specific heat of the mashed potatoes as described by Sablani et al. (2009). The 15–20 mg sample was sealed in an aluminum pan and equilibrated at 20 °C for 5 min. The sample was then scanned to 125 °C at the rate of 5 °C/min before being equilibrated back to 20 °C for 10 min. The experiments were performed in triplicate. The specific heats of pea and rice were obtained from Jain et al. (2019).

2.2.2. Processing using MAPS

Mashed potato samples were processed with the MAPS to validate the charts. Samples of 280 g and 22 mm thick (area: 140 × 95 mm) were filled into 310.5 mL (10.5 oz) single-serve retort trays; samples of 340 g and 28 mm thick (area: 140 × 95 mm) were filled into 443.6 mL (15 oz) retort trays, and samples of 1850 g and 30 mm thick (area: 290 × 230 mm) were poured into 2100 mL (71 oz) institutional retort trays. All of the samples had 0 or 0.6% salt content. The trays were vacuum sealed (6.5 kPa) with a Multivac T-200 sealer (Multivac Inc., Kansas City, MO, USA). For temperature measurement, a mobile metallic sensor (Ellab Inc., Hillerod, Denmark) was embedded in the food sample with its tip located at the cold spot, as described by Luan et al. (2015, 2013). The cold spot locations were identified with preliminary MAPS runs and experimental heating pattern tests (Hong et al., 2021).

The generator power setup was 5 kW each for the first two cavities and 8.7 kW for the third and fourth cavities combined (Fig. 1). Due to power reflection, a total net power of 10 ± 0.2 kW (an average 2.5 kW for each cavity) was applied in the microwave heating section. It should be noted that some of the net power was also be absorbed by the circulating water before reaching the packaged food. In pasteurization, the samples in a food package carrier were loaded into the preheating section and heated to 51 °C in warm circulating water. The samples were then moved through the microwave heating section. The reverse osmosis purified circulating water was set at 91 °C, and the residence time for the samples to travel through the four interconnected horn applicators in the microwave heating cavity was 3.3 min (89 cm/min) for 22 and 28 mm products and 4 min (71 cm/min) for 30 mm products. The samples were then held for 2 min in the holding section, where the circulating water temperature was also set at 91 °C. Finally, the samples were moved into the cooling section to reach 23 °C. The experimental runs for the packaged samples were conducted in duplicates.

2.3. Statistical analysis

In the chart development and statistical analyses, MATLAB with Statistics Toolbox software version 2020b (Natick, MA, USA) was utilized. The adequacy of the correlation between the predicted and the experimental temperature values were determined by evaluating the lack of fit, the coefficient of determination (R^2) and the Root Mean Square Deviation (RMSD) of the linear regression. As Piñeiro et al. (2008) suggested, the experimental values (y-axis) were plotted against the predicted values (x-axis) for the regressions. The statistical significance of the models and standardized residuals were evaluated at the 5% probability level ($P < 0.05$).

3. Results and discussion

3.1. Chart development

3.1.1. Relationship between temperature and the dielectric properties of food samples

Firstly, the relationship between temperature and the dielectric loss factor was established at different salt contents (Table 1). These relations are illustrated in Fig. 3 for mashed potato samples. Fig. 3 shows the rise of the loss factor in mashed potatoes with increased dissolved salt and temperature. This is due to the increased ionic conductivity of the dissolved ions from the added salt and the temperature enhanced mobility of the charged ions (İcier and Baysal, 2004; Ryynänen, 1995; Tang, 2015). A similar observation is also obtained for pea and rice products (Figs. 7 and 8), except for the rice samples with 0% salt content, which are transparent for microwaves (Jain et al., 2019).

Table 2 shows the relationships between temperature and the dielectric constant of three food samples with different salt contents. The relationships shown in Tables 1 and 2 allow the prediction of the dielectric properties for the three products at different temperatures and salt contents. These relationships were used in developing the first half of a comprehensive chart that relates heating rates to product properties and sample thickness.

3.1.2. The relationships among heating rate, dielectric properties, package thickness

Fig. 4 shows the flowchart used in MATLAB software to predict the heating rate of products as it is influenced by product temperature and dielectric properties. Eqs. (2) and (10) were used to determine the central layer electric field intensity (E) and power dissipation (P), respectively, for different salt contents and package thicknesses (16, 18, 20, 22, 25, 28, 30, 35 and 40 mm). Once the power dissipation at the central layer of the food tray was determined, the heating rate was calculated using Eq. (11). The volumetric specific heat was 3.6, 4.7 and 3 MJ/(°C.m^3) for mashed potato, pea and rice products, respectively. The sample density was 1×10^3, 1.3×10^3 and 0.96×10^3 kg/m^3, respectively.

Using Eq. (12) (derived from Eqs. (10) and (11)), the loss factors (y-axis) of the mashed potatoes were plotted against the calculated heating

Table 1
Relationships between temperature and the dielectric loss factor at different salt contents.

Salt content (added salt)	Correlations	R^2
Mashed Potatoes		
0.0%	$\varepsilon'' = 1 \times 10^{-3} \times T^2 - 0.0264 \times T + 14.22$	0.99
0.1%	$\varepsilon'' = 2.3 \times 10^{-3} \times T^2 - 0.0984 \times T + 19.51$	0.99
0.6%	$\varepsilon'' = 3.4 \times 10^{-3} \times T^2 - 0.0019 \times T + 29.74$	0.99
1.0%	$\varepsilon'' = 3.7 \times 10^{-3} \times T^2 + 0.1675 \times T + 36.64$	0.99
1.5%	$\varepsilon'' = 7 \times 10^{-3} \times T^2 + 0.0361 \times T + 52.05$	0.99
2.0%	$\varepsilon'' = 5.8 \times 10^{-3} \times T^2 + 0.3851 \times T + 54.18$	0.99
Peas		
0.0%	$\varepsilon'' = -2 \times 10^{-4} \times T^2 + 0.1529 \times T + 5.72$	0.99
0.1%	$\varepsilon'' = 2 \times 10^{-4} \times T^2 + 0.1360 \times T + 9.28$	0.99
0.2%	$\varepsilon'' = 2 \times 10^{-4} \times T^2 + 0.1904 \times T + 10.63$	0.99
0.5%	$\varepsilon'' = 7 \times 10^{-4} \times T^2 + 0.2386 \times T + 16.13$	0.99
1.0%	$\varepsilon'' = 1.2 \times 10^{-3} \times T^2 + 0.3361 \times T + 27.42$	0.99
2.0%	$\varepsilon'' = -1 \times 10^{-3} \times T^2 + 0.9162 \times T + 32.81$	0.97
Rice		
0.0%	$\varepsilon'' = 2 \times 10^{-4} \times T^2 - 0.0307 \times T + 7.54$	0.98
0.2%	$\varepsilon'' = 4 \times 10^{-4} \times T^2 - 0.0181 \times T + 7.81$	0.99
0.5%	$\varepsilon'' = -3 \times 10^{-4} \times T^2 + 0.0623 \times T + 9.43$	0.99
1.0%	$\varepsilon'' = 4 \times 10^{-5} \times T^2 + 0.1571 \times T + 11.85$	0.99
1.5%	$\varepsilon'' = -7 \times 10^{-6} \times T^2 + 0.3444 \times T + 14.58$	0.99
2.0%	$\varepsilon'' = -6 \times 10^{-5} \times T^2 + 0.6508 \times T + 16.23$	0.99

T = temperature (°C), (n = 3).

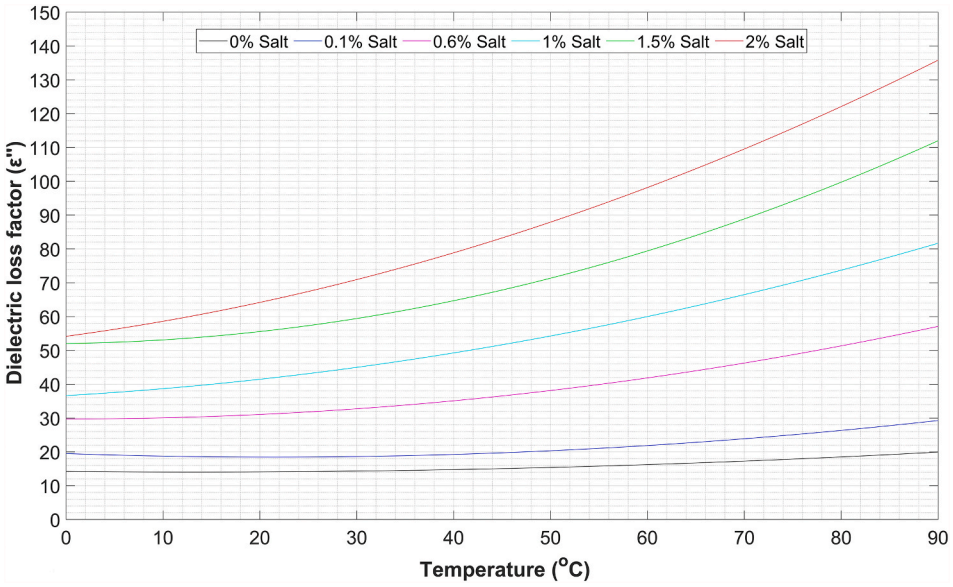

Fig. 3. Relationships between temperature and the dielectric loss factor at different salt contents of mashed potatoes.

Table 2
Relationships between temperature and the dielectric constant at different salt contents.

Salt content (added salt)	Correlations	R^2
Mashed Potatoes		
0.0%	$\varepsilon' = -7 \times 10^{-4} \times T^2 - 0.1148 \times T + 81.00$	0.99
0.1%	$\varepsilon' = -4 \times 10^{-4} \times T^2 - 0.1589 \times T + 82.19$	0.99
0.6%	$\varepsilon' = -9 \times 10^{-4} \times T^2 - 0.0698 \times T + 77.96$	0.99
1.0%	$\varepsilon' = -4 \times 10^{-4} \times T^2 - 0.1163 \times T + 78.51$	0.99
1.5%	$\varepsilon' = -1.1 \times 10^{-3} \times T^2 - 0.0332 \times T + 78.22$	0.99
2.0%	$\varepsilon' = -4 \times 10^{-4} \times T^2 - 0.0753 \times T + 75.57$	0.99
Peas		
0.0%	$\varepsilon' = -1 \times 10^{-4} \times T^2 - 0.0714 \times T + 59.43$	0.99
0.1%	$\varepsilon' = 4 \times 10^{-4} \times T^2 - 0.1325 \times T + 59.13$	0.99
0.2%	$\varepsilon' = 8 \times 10^{-4} \times T^2 - 0.2289 \times T + 65.92$	0.99
0.5%	$\varepsilon' = 1 \times 10^{-4} \times T^2 - 0.0979 \times T + 62.66$	0.99
1.0%	$\varepsilon' = 0 \times 10^{-4} \times T^2 - 0.0657 \times T + 61.00$	0.99
2 .0%	$\varepsilon' = 3 \times 10^{-4} \times T^2 - 0.1068 \times T + 61.70$	0.99
Rice		
0.0%	$\varepsilon' = 4 \times 10^{-4} \times T^2 - 0.1635 \times T + 65.45$	0.99
0.2%	$\varepsilon' = 6 \times 10^{-4} \times T^2 - 0.2193 \times T + 65.78$	0.99
0.5%	$\varepsilon' = 6 \times 10^{-4} \times T^2 - 0.2250 \times T + 69.65$	0.99
1.0%	$\varepsilon' = 8 \times 10^{-4} \times T^2 - 0.2471 \times T + 67.37$	0.99
1.5%	$\varepsilon' = -4 \times 10^{-4} \times T^2 - 0.0632 \times T + 62.19$	0.99
2.0%	$\varepsilon' = -1 \times 10^{-4} \times T^2 - 0.0907 \times T + 67.04$	0.99

T = temperature (°C), (n = 3).

rates (x-axis) for different salt contents and thicknesses to create the second half of the chart, as shown in Fig. 5. In this figure, the black dashed lines are drawn with fixed dielectric constant values that range from 60 to 80 with an interval of 5 (60:5:80). These fixed lines can be used as a reference to track the change in the dielectric constant values as the temperature increases. For peas and rice, the dashed lines are from 45 to 65 (45:5:65).

$$\varepsilon'' = \frac{\rho C_P}{2\pi f \varepsilon_o |E|^2}\left(\frac{dT}{dt}\right) \tag{12}$$

3.1.3. Formation of the final charts

Finally, the graphs in Figs. 3 and 5 were superimposed using MATLAB software to form the chart shown in Fig. 6 for mashed potatoes. Eq. (13) shows how the equations from Table 1 and Eq. (12) are related to

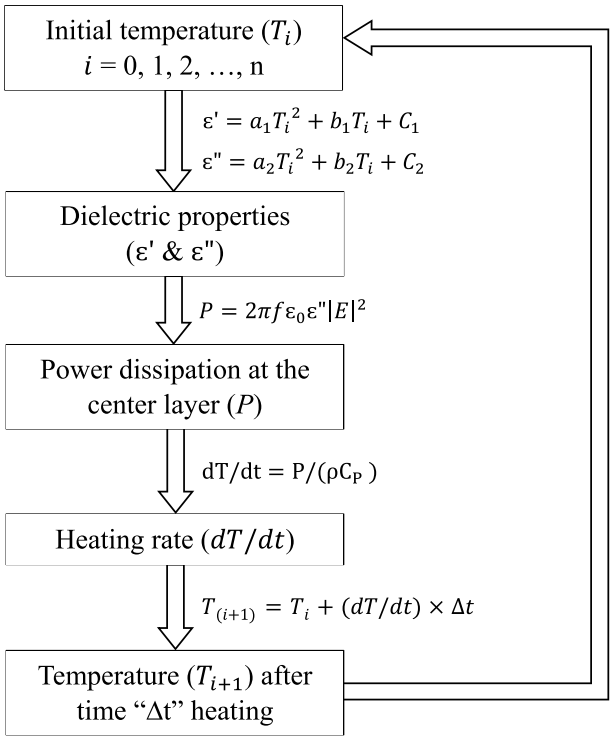

Fig. 4. Loop iteration for the heating rate prediction.

establish a connection between the product heating temperature (T) and heating rate (dT/dt). A similar approach was applied to create Figs. 7 and 8 for pea and rice products, respectively. The newly developed analytical charts are named as Gezahegn-Tang (G-T) charts. The G-T charts shed light on the complex relationships among dielectric constant, loss factor, food temperature, salt content, thickness, and heating rate in the central layer of the food processed in the MAPS. In reading the charts, the loss factor *vs.* temperature lines from the first half graph (the black horizontal axis on top of the chart) and the loss factor *vs.* heating rate curves from the second half graph (the blue horizontal axis on the bottom of the chart) must go together according to the respective colors that indicate salt contents. The short heating rate curves near the left

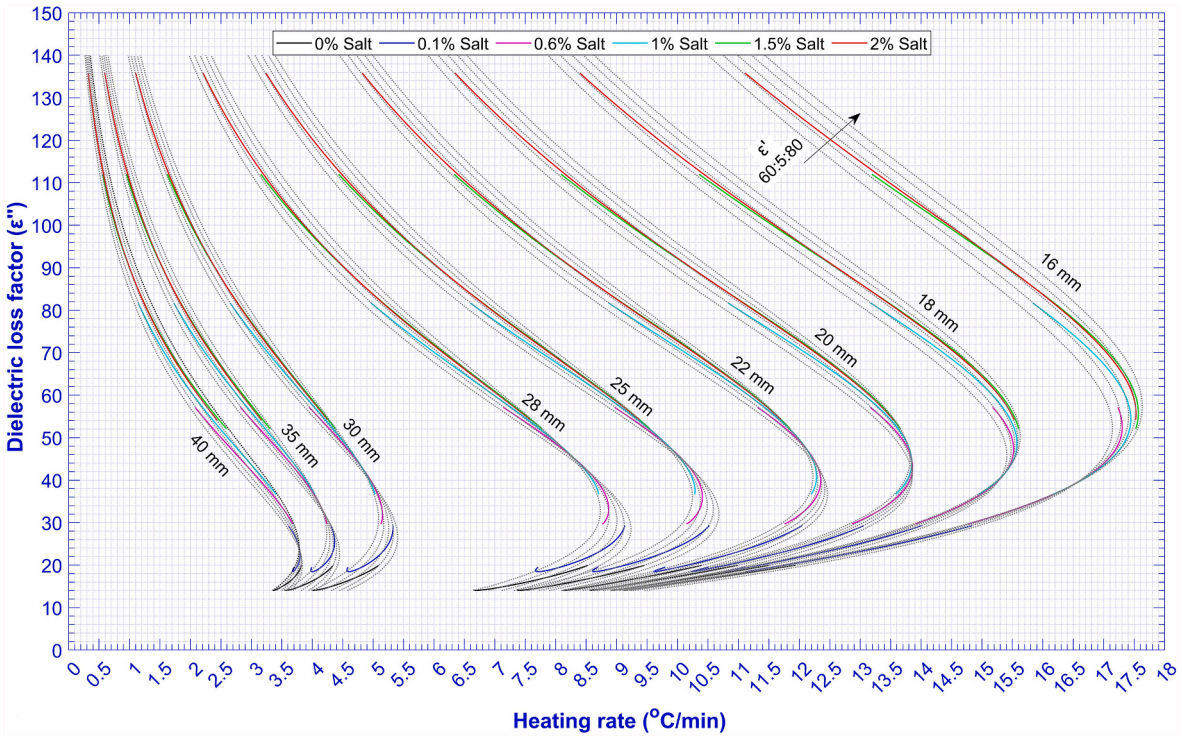

Fig. 5. Relationships among the dielectric properties, thickness, and heating rate at different salt contents in mashed potatoes during heating with the MAPS.

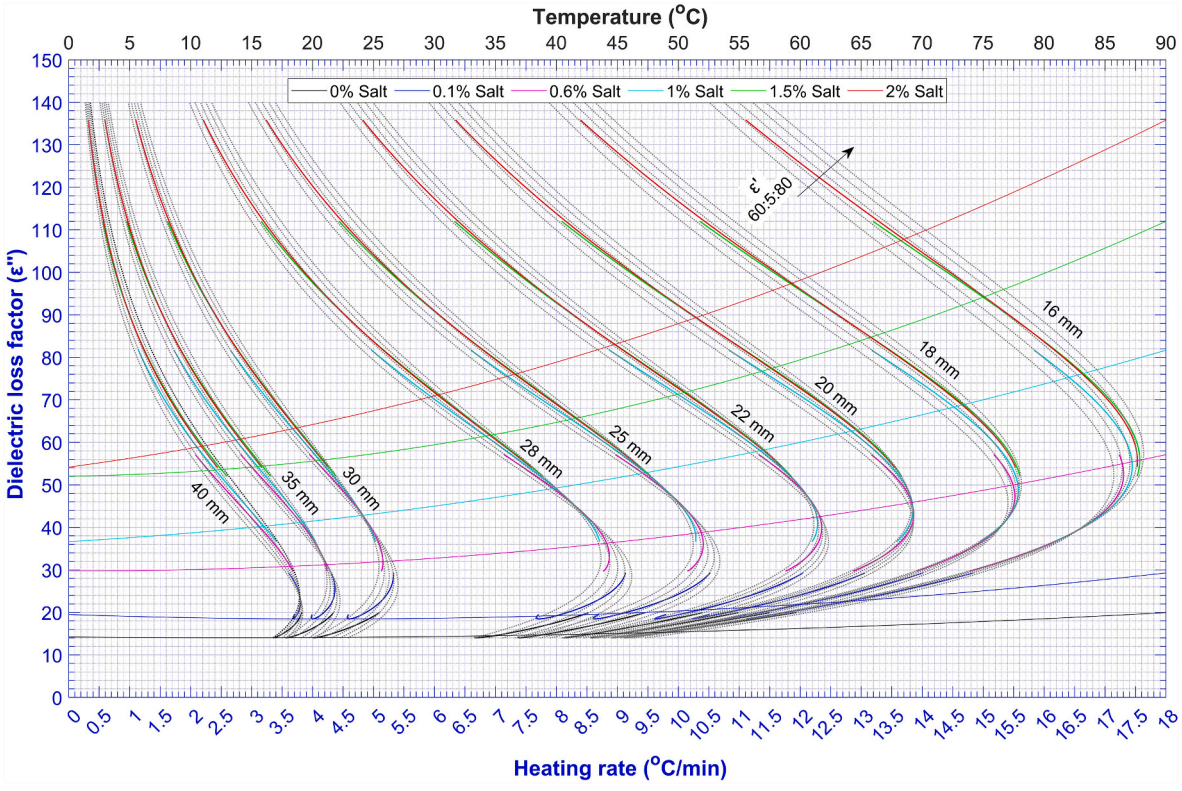

Fig. 6. G-T chart for the mashed potato samples in the MAPS.

bottom corner of Fig. 8 indicate that the rice samples with 0% salt content have very low heating rates at the center. Similar observations, lower heating rate and loss factor, were also reported by Jain et al. (2019) and Auksornsri et al. (2018).

$$\underbrace{aT^2 + bT + c = \varepsilon''}_{\text{First half of the G–T chart}} = \underbrace{\frac{\rho C_P}{2\pi f \varepsilon_o |E|^2}\left(\frac{dT}{dt}\right)}_{\text{Second half of the G–T chart}} \tag{13}$$

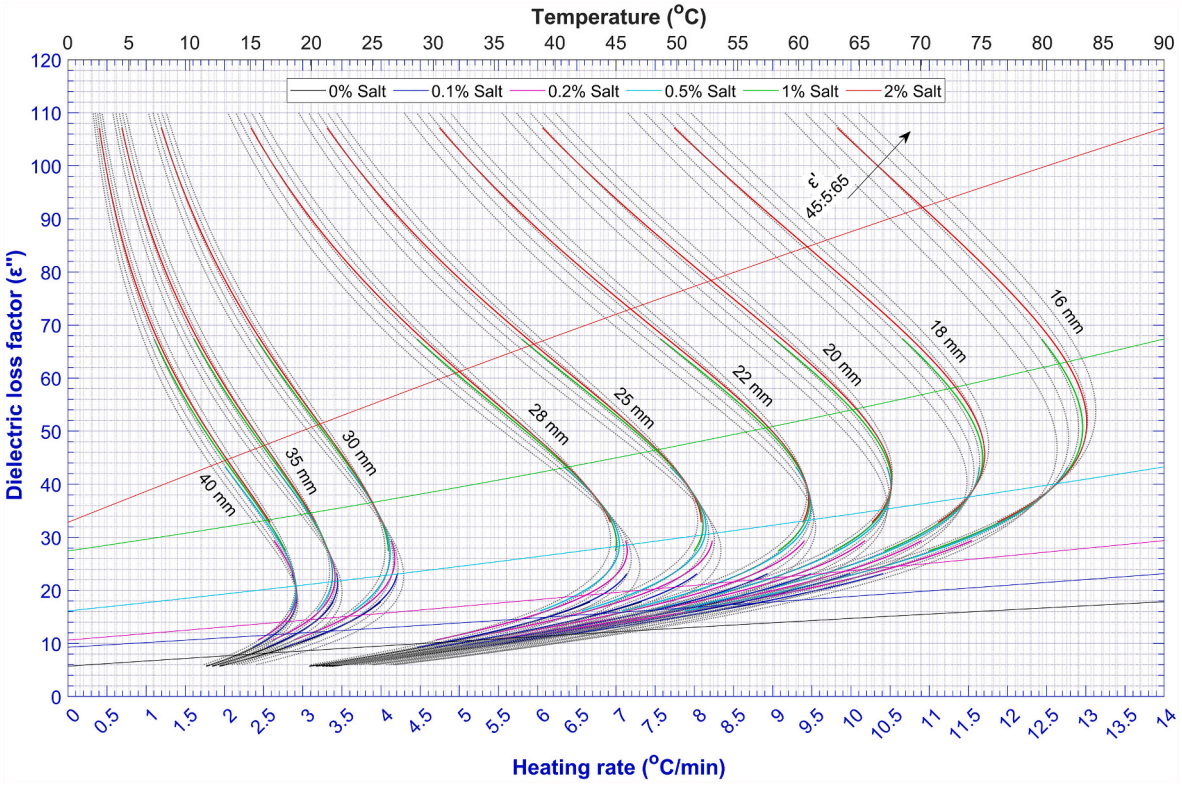

Fig. 7. G-T chart for the pea samples in the MAPS.

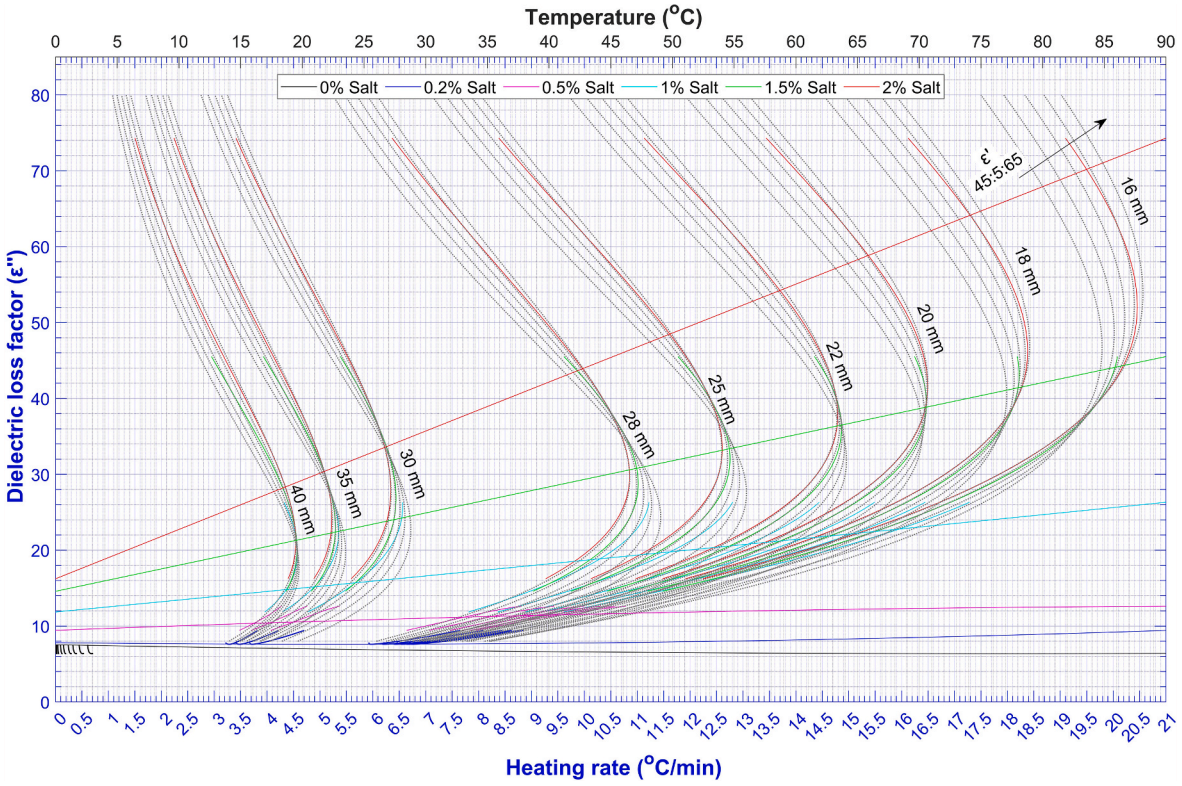

Fig. 8. G-T chart for the rice samples in the MAPS.

3.2. Chart validation

3.2.1. Product temperature

Mashed potato samples with different salt contents (0 & 0.6%) and thicknesses (22, 28 and 30 mm) were processed with the MAPS to validate the accuracy of the chart predictions. The chart prediction was based on the loop iteration presented in Fig. 4. For calculating the predicted values, T_i was set to match the experimental preheating temperature (51 °C) of the product, and the iterative calculations were made with a 2-s interval same as the sensor recording time interval used for the experiment. The predicted cold-spot temperatures are compared in Fig. 9 with the corresponding experimental values measured by mobile temperature sensors placed in the central layer of the samples. In each experimental test, 99 data observations were recorded within 3.3 min of microwave heating. The predicted temperature rises are in general agreement with the experimental temperatures presented in Fig. 9 within the 95% confidence interval, with R^2 from 0.96 to 0.99. Furthermore, more than 95% of the standardized residuals are between the −2 and 2 °C range. Thus, the G-T chart can accurately predict temperatures at the central layer of the food samples with various salt contents and thicknesses.

The wavy pattern in the experimental temperatures in Fig. 9 reflects food package movement between the horn applicators through the microwave heating cavities. The maximum microwave heating (electric field intensity) occurs at the center of the horn applicators (perpendicular to the microwave source), whereas the minimum microwave heating occur at the entrance and exit of the horn applicators (Luan et al., 2016). It is, therefore, expected that food packages received maximum power when traveling between each pair of the horn applicators of the four microwave heating sections illustrated in Fig. 1, while our prediction assumed a uniform microwave energy (average electric field intensity) exposure over the 3.3 min heating time.

3.2.2. Average heating rate

The average heating rates of the predicted and experimental values of the mashed potatoes with different thicknesses and salt contents were compared. The average heating rates were determined by dividing the differences between the final and the preheating temperatures by the heating time (3.3 min). As depicted in Fig. 10, in both predicted and experimental observations, samples with less thickness (22 mm) were heated faster than the thicker samples (28 and 30 mm). In addition, the increase of the salt content from 0 to 0.6% increased the heating rate. The results in Fig. 10 show an agreement between the predicted and experimental heating rate values.

3.3. The G-T chart applications

3.3.1. Determining dielectric properties

The dielectric loss factors (ε") can be seen in the first half of the G-T chart (Figs. 6, 7 or 8) that relates the temperature with the loss factor. To read the loss factors of a food sample with a known temperature and salt content, users first locate the temperature on the top axis, then move vertically downward until the intersection with the curve for the corresponding salt content, and then read the value of the dielectric loss factor from the left axis. Two examples are presented in Fig. 11 by arrows. Arrows "a-1" and "a-2" show that a mashed potato sample at 70 °C and with 1.5% salt content has a loss factor of 89. Similarly, arrows "b-1" and "b-2" show at 90 °C and with 2% salt content, the loss factor is 136.

The dielectric constant (ε') of a food sample with a known temperature and salt content can also be read in the G-T chart shown in Fig. 11. In reading, users start from the temperature of the food sample (70 or 90 °C), move downward until the intersection with the specific salt content (1.5 or 2%) loss factor *vs*. temperature line, then move horizontally until the intersection with the corresponding loss factor *vs*. heating rate curve (green or red color) that relates to the corresponding salt content. The dielectric constant value can be obtained by referring to the black dashed lines. As depicted in Fig. 11, by following arrows "a-1″ and "a-2″, the dielectric constant of the mashed potato sample at 70 °C and with 1.5% salt content can be read 70 from the third dashed line. Similarly, for the sample at 90 °C and with 2% salt content, users can refer to arrows "b-1″ and "b-2″ to read the dielectric constant value of 65 from the second dashed line. Since the dielectric constants and loss factors are not a function of thickness in a homogeneous food, users can refer to their values regardless of the sample thickness in the chart.

3.3.2. Determining heating rate

The G-T chart predicts the heating rate at a certain temperature, given the salt content and thickness of the food. From the first half of the charts in Figs. 6, 7 or 8, users can relate a specific temperature of a food sample with its loss factor, as described in Section 3.3.1. Then, by referring to the loss factor, users can obtain the corresponding heating rate from the second half of the charts. In reading the chart in Fig. 12, one would start from the temperature of the food sample and move downward (arrow a-1 or b-1) until the intersection with the loss factor *vs*. temperature curve for the specific salt content. Afterward, moving horizontally (arrow a-2 or b-2) until the intersection with the corresponding loss factor *vs*. heating rate curve of the specific thickness and salt content and then moving downward (arrow a-3 or b-3) leads to the value of the heating rate from the blue bottom horizontal axis. Therefore, a mashed potato sample at 30 °C temperature with 2% salt content and 22 mm thick would have a heating rate of 10.17 °C/min. Similarly, for a sample at 60 °C with 0.6% salt content and 30 mm thick, the heating rate would be 4.87 °C/min.

3.3.3. Determining the optimal preheating temperature

The optimal preheating temperature for the maximum microwave heating rate can be determined for a given food thickness and salt content. During heating from preheating temperature to the desired pasteurization temperature (70–90 °C), the corresponding heating rate curve shall include the maximum (peak) heating rate. Thus, the maximum microwave energy will be utilized during the process. Starting the heating lower from the vertex (maximum) of the heating rate curve is recommended for preheating temperature determination. If we select the maximum as a starting point, the heating will begin from the maximum heating rate and drop to the lower heating rates as the heating progresses.

The two examples in Fig. 13 show that the optimal preheating temperature can be obtained by identifying the maximum heating rate for a specific food thickness and salt content. From the identified point (lower from the Max) on the heating rate curve, moving horizontally (arrow a-1 or b-1) until the intersection with the loss factor *vs*. temperature line of the identical salt content, then moving vertically upward (arrow a-2 or b-2) leads to the optimal temperature from the top axis. The optimal preheating temperature is recommended for attaining the product's maximum microwave heating rate. In the example with arrows b-1 and b-2, a mashed potato sample with 0.6% salt content and 20 mm thickness has an optimal preheating temperature of 45 °C.

To ensure that the selected optimal preheating temperature accommodates the maximum heating rate during the heating, we can use Eq. (14) to determine the final heating temperature ($T_{(Final)}$):

$$T_{(Final)} = T_{(Opt)} + \left(dT/dt_{(Opt)} \times t\right) \tag{14}$$

where $T_{(Opt)}$ is the optimal preheating temperature, $dT/dt_{(Opt)}$ is the heating rate at the selected optimal preheating temperature (lower from the vertex), and t is the heating time.

For the example (b-1 and b-2) with 3.3 min heating time, $T_{(Final)}$ will be 90 °C (Eq. (14)):

$$T_{(Final)} = 45\,^{\circ}C + (13.65\,^{\circ}C/\text{min} \times 3.3\ \text{min})$$

The product temperature at the maximum heating rate (vertex) is

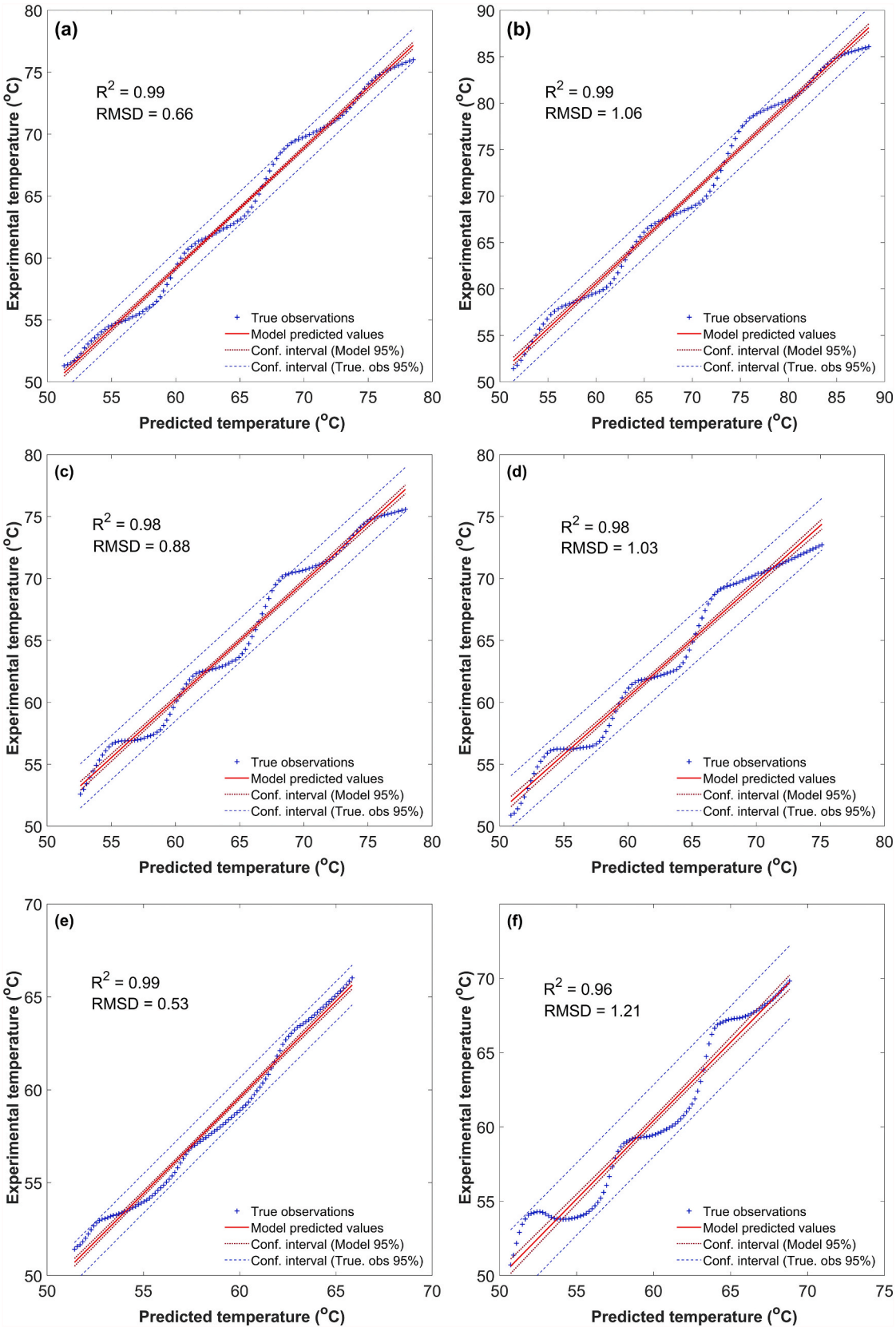

Fig. 9. Correlation between the experimental and predicted temperatures in the center layer of mashed potatoes 22 mm thick with 0% (a) and 0.6% (b) salt contents; 28 mm thick with 0% (c) and 0.6% (d) salt contents, and 30 mm thick with 0% (e) and 0.6% (f) salt contents. The central line corresponds to the regression model of the predicted temperatures; the dotted lines (..) represent the 95% confidence interval for the regression, and the dashed lines (– –) represent the 95% confidence interval for the experimental values.

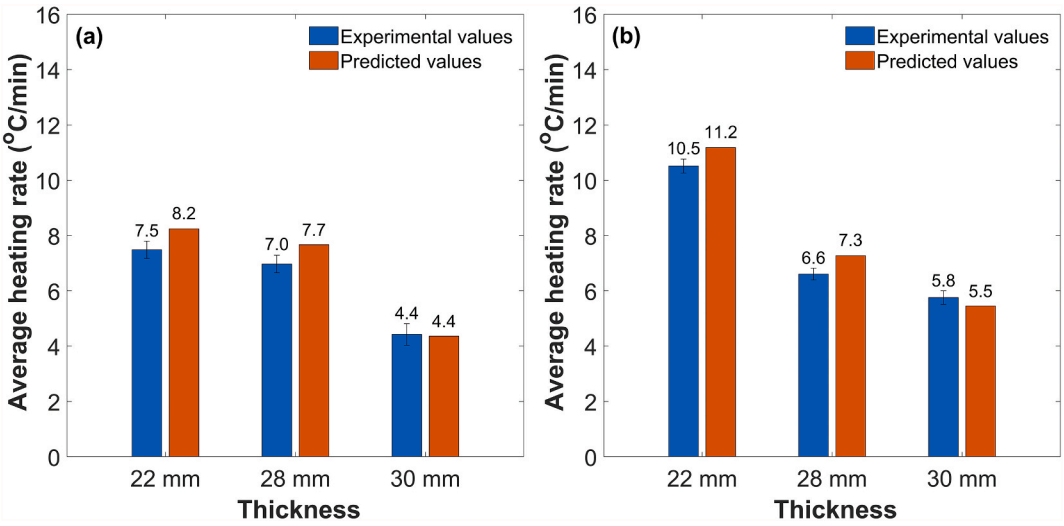

Fig. 10. The average heating rates at different thicknesses and with 0% (a) and 0.6% (b) salt contents.

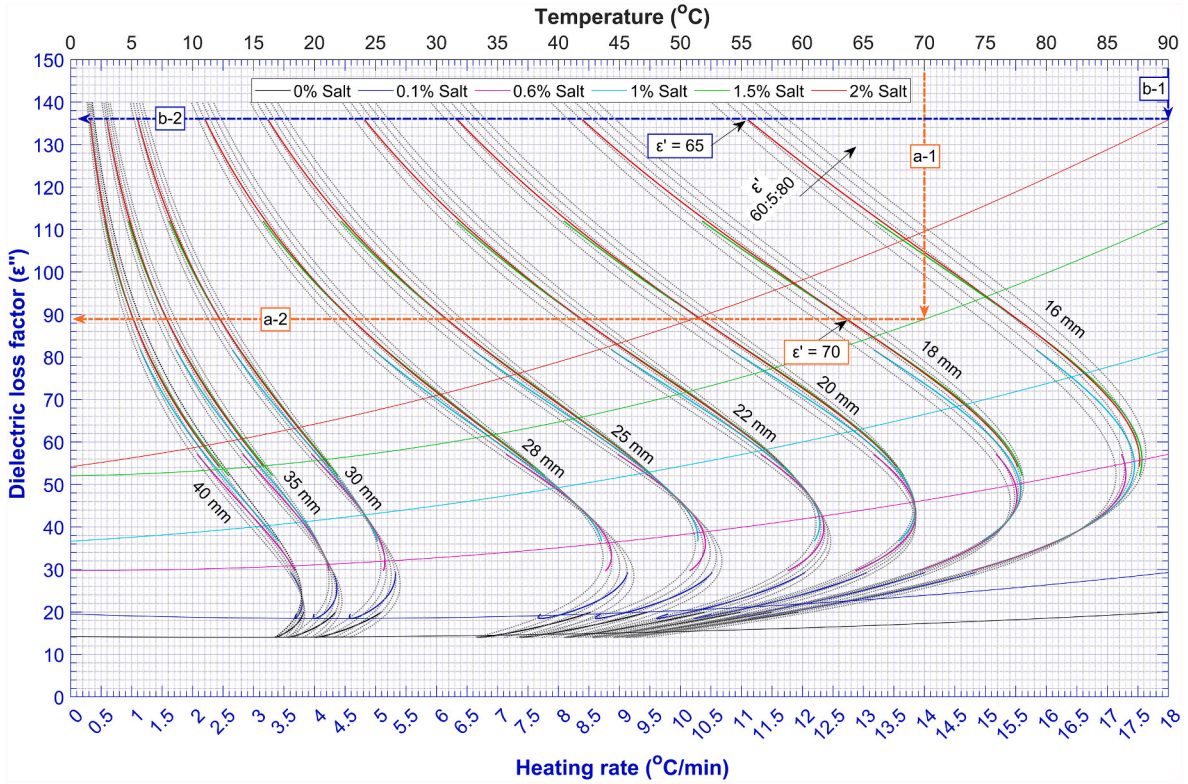

Fig. 11. Dielectric property determination of the mashed potato samples.

63 °C, which can be found with the same approach as arrows b-1 and b-2 by starting b-1 at the maximum heating rate. Since the final heating temperature (90 °C) is above the temperature (63 °C) of the product at its maximum heating rate, we can conclude that starting the heating process at the selected optimal preheating temperature (45 °C) can accommodate the maximum heating rate during the heating process.

In the example with arrows a-1 and a-2, the heating rate curve is a relatively straight line with a positive slope. Since the microwave heating rate increases linearly, we can select the optimal heating temperature at a point that will not damage the product quality. In the example for mashed potatoes with 0.1% salt content and 25 mm thickness, if we select 50 °C as an optimal preheating temperature, the final product temperature after 3.3 min heating will be 80 °C (Eq. (14)):

$$T_{(Final)} = 50\,^{\circ}C + (9.15^{\circ}C\,/\,\text{min} \times 3.3\ \text{min})$$

This approach allows the effective utilization of microwave energy at the product's optimal temperature. For products with lower optimal preheating temperatures and that do not reach the final pasteurization temperature after microwave heating, the pasteurization can be completed with circulating hot water in the holding section. Alternatively, a longer microwave heating time can be used in the heating section. In general, increasing the salt content (loss factor) results in a reduction of the optimal preheating temperature.

Although the G-T charts were designed for homogenous and single

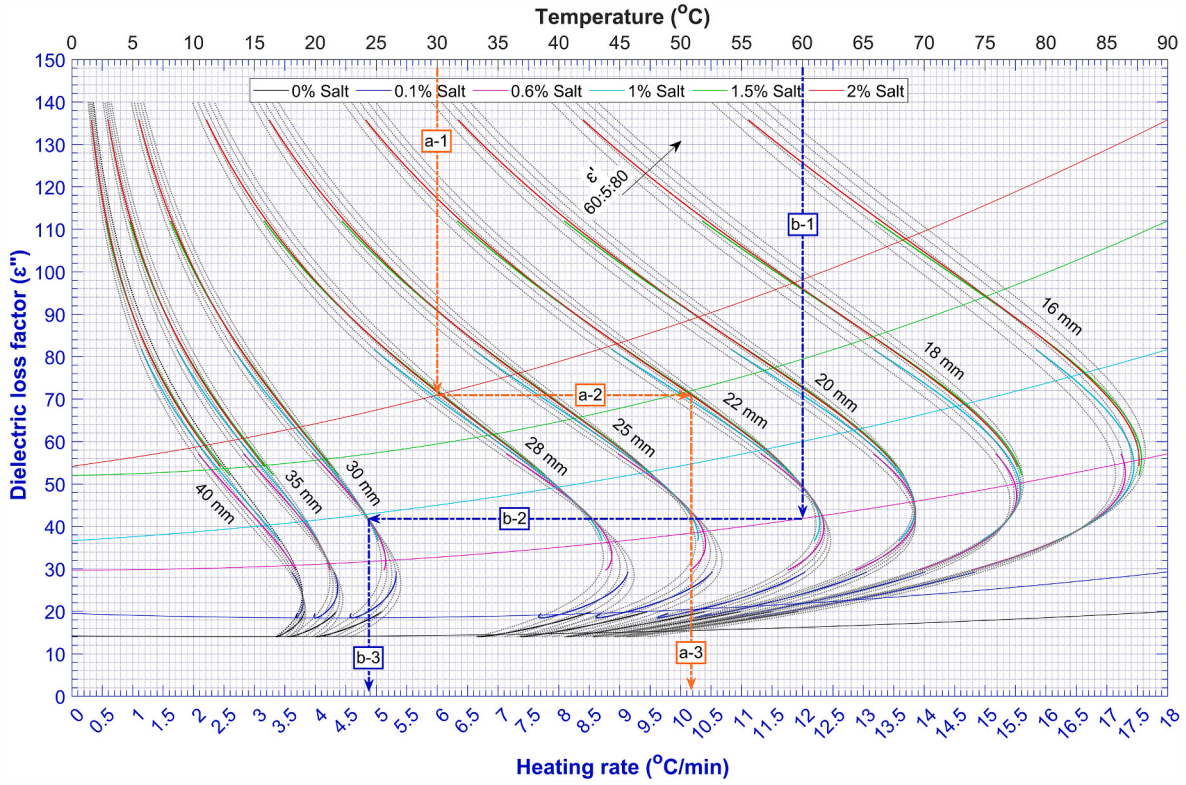

Fig. 12. Heating rate determination of the mashed potato samples in the MAPS.

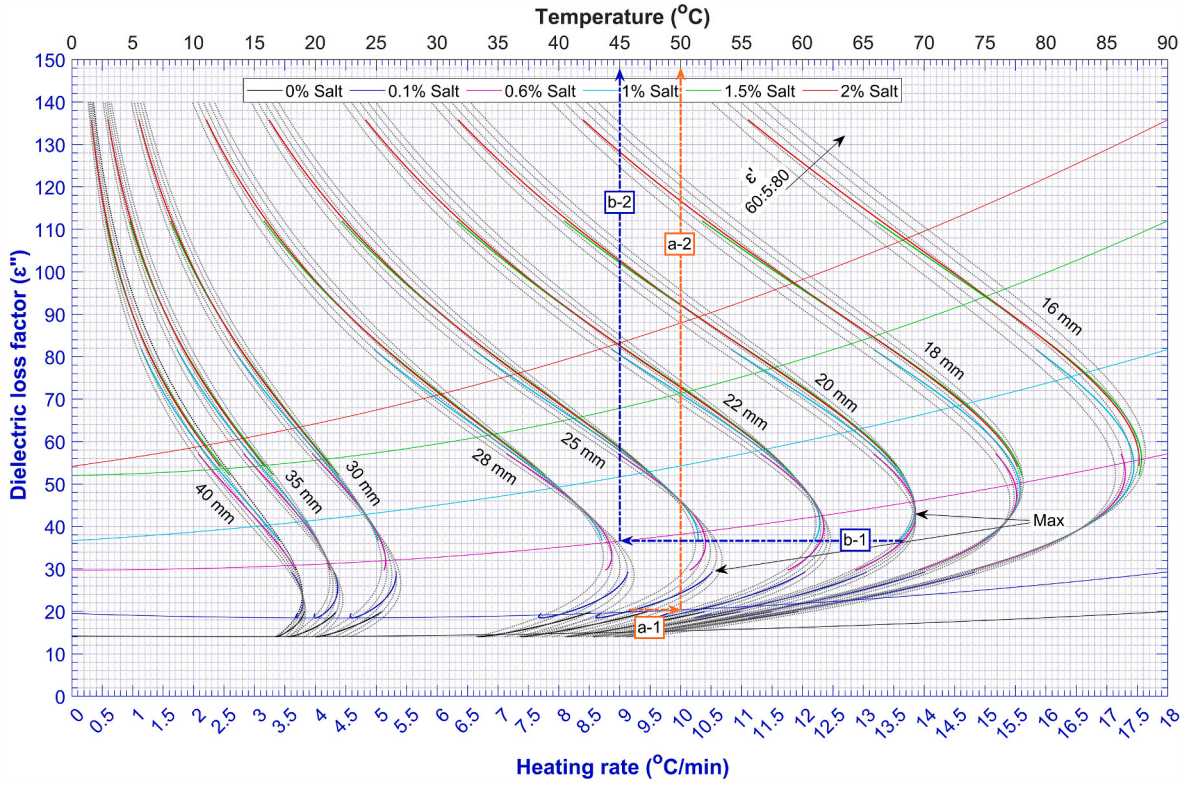

Fig. 13. Optimal preheating temperature determination of the mashed potato samples in the MAPS.

compartment foods, they can be applied for multi-compartment trays in three different manners. The first application is to estimate the heating rate of the least heated compartment. This is done by finding the average heating rate of the individual food components, and then the ingredient with the lowest average heating rate can be used as a worst-case scenario. The average heating rate can be determined by taking the mean value within the heating rate range (between the heating rates obtained at the initial/preheating temperature to the final temperature). For instance, in pasteurizing a 22 mm thick (10 oz) multi-compartment food containing mashed potatoes (1% salt), peas (0.5% salt) and rice (0.5% salt) samples, from preheating temperature of 50–90 °C, a manufacturer can identify that pea have the lowest average heating rate (9.30–9.50 °C/min) (Fig. 7) relative to mashed potatoes (8.87–11.67 °C/min) (Fig. 6) and rice (9.13–10 °C/min) (Fig. 8) samples. In this case, the pea can be considered as the worst-case scenario in process schedule development. The second application is to adjust compartment thickness to obtain relatively uniform heating in multi-compartment trays. For example, having 22 mm mashed potato, 20 mm pea and 28 mm rice with 1% salt content in each compartment gives a relatively close average heating rate that ranges from 8.87 to 11.67, 9.02–10.38 and 10.51–11.22 °C/min, respectively. The third application is to adjust the salt content in different compartments to obtain relatively uniform heating. For example, by changing the salt content (while keeping the 22 mm thickness) to 0% in mashed potatoes and 0.5% in peas and rice samples, it is possible to obtain heating rates of 8.77–10.41, 9.30–9.50 and 9.13–10 °C/min, respectively, which are relatively close.

If the input power from the generators has changed, the E_0 shall be determined to get an accurate estimation of the heating rate. According to Eq. (10), a change in the E_0 value will alter the heating rate by the power of two. To use the G-T chart for different systems other than the MAPS used in this study, the first half of the chart (loss factor *vs.* temperature lines) can be used as it is, yet for the second half of the chart (loss factor *vs.* heating rate curves), the E_0 needs to be determined by simulation software or from experimental results. Eqs. (13) and (2) can be used to experimentally determine the average E and E_0, respectively, by measuring the heating temperature (T), heating rate (dT/dt), dielectric properties and volumetric specific heat of the food.

4. Conclusions

Three distinct charts for mashed potato, pea and rice samples were developed to show the relationships among the dielectric properties, preheating temperature, thickness, and heating rate at the cold spots of food samples in microwave heating with the MAPS. From the G-T charts, users can acquire four main types of information: loss factor, dielectric constant, optimal preheating temperature and heating rate for the selected products processed in the MAPS. The chart for mashed potato samples was validated by experimental microwave heating tests with the 915 MHz single-mode MAPS system at Washington State University. The predicted and experimental temperature profiles at the cold spots of the mashed potato samples agreed well with higher R^2 (0.99–0.96). Few thicker samples (>30 mm) showed lower R^2 (0.96); however, more than 95% of the standardized residuals were between the −2 and +2 range in all samples. Further research is needed to validate the charts for rice and peas. Additionally, similar G-T charts can be developed for various food products. The findings from this research can be integrated with the pilot-scale or commercial MAPS process control systems to assist the process schedule development. Web-based or Non-web-based automation and control software can be developed to integrate the concept of the G-T charts. Using the G-T charts can significantly save time and resources in food product and MAPS process developments in the food industry.

Credit author statement

Yonas A. Gezahegn: Conceptualization, Methodology, Investigation, Validation, Data Curation and analysis, Software, Writing - Original Draft, Visualization and Project administration. **Yoon-Ki Hong**: Investigation, Writing - Reviewing and Editing. **Juming Tang**: Conceptualization, Methodology, Writing - Review & Editing, Funding acquisition, Resources, Supervision and Project administration. **Patrick D. Pedrow**: Conceptualization, Writing - Reviewing and Editing. Shyam S. Sablani: Conceptualization, Writing - Reviewing and Editing, **Fang Liu**: Investigation and Data Curation. **Zhongwei Tang**: Investigation, Data Curation, Writing- Reviewing and Editing.

Declaration of competing interest

- All authors have participated in (a) conception and design, or analysis and interpretation of the data; (b) drafting the article or revising it critically for important intellectual content; and (c) approval of the final version.
- This research article is original, and neither submitted nor under review for publication elsewhere.
- Its publication is approved by all authors and tacitly or explicitly by the responsible authorities where the work was carried out and sponsored.
- If accepted, it will not be published elsewhere in the same form, in English or in any other language, including electronically without the written consent of the copyright-holder.

Data availability

Data will be made available on request.

Acknowledgments

The authors would like to acknowledge the USDA: National Institute of Food and Agriculture grant (#2016-68003-24840) and Washington State University: Hatch project (#1016366).

Appendix A. Supplementary data

Supplementary data to this article can be found online at https://doi.org/10.1016/j.jfoodeng.2023.111434.

References

Auksornsri, T., Tang, J., Tang, Z., Lin, H., Songsermpong, S., 2018. Dielectric properties of rice model food systems relevant to microwave sterilization process. Innovat. Food Sci. Emerg. Technol. 45, 98–105. https://doi.org/10.1016/j.ifset.2017.09.002.

FDA, 2016. Center for Food Safety and Applied Nutrition. Hazard Analysis and Risk-Based Preventive Controls for Human Food: Guidance for Industry. Department of Health and Human Services.

Balanis, C.A., 2012. Advanced Engineering Electromagnetics, second. John Wiley & Sons, Inc., NJ.

Bornhorst, E.R., Tang, J., Sablani, S.S., Barbosa-Cánovas, G.V., 2017. Development of model food systems for thermal pasteurization applications based on Maillard reaction products. LWT 75, 417–424. https://doi.org/10.1016/j.lwt.2016.09.020.

Chandrasekaran, S., Ramanathan, S., Basak, T., 2013. Microwave food processing - a review. Food Res. Int. 52, 243–261. https://doi.org/10.1016/j.foodres.2013.02.033.

Chen, H., Tang, J., Liu, F., 2008. Simulation model for moving food packages in microwave heating processes using conformal FDTD method. J. Food Eng. 88, 294–305. https://doi.org/10.1016/j.jfoodeng.2008.02.020.

Gezahegn, Y.A., Tang, J., Sablani, S.S., Pedrow, P.D., Hong, Y.-K., Lin, H., Tang, Z., 2021. Dielectric properties of water relevant to microwave assisted thermal pasteurization and sterilization of packaged foods. Innovat. Food Sci. Emerg. Technol. 74, 102837 https://doi.org/10.1016/j.ifset.2021.102837.

Hong, Y.-K., Liu, F., Tang, Z., Pedrow, P.D., Sablani, S.S., Yang, R., Tang, J., 2021. A simplified approach to assist process development for microwave assisted pasteurization of packaged food products. Innovat. Food Sci. Emerg. Technol. 102628 https://doi.org/10.1016/j.ifset.2021.102628.

İcier, F., Baysal, T., 2004. Dielectrical properties of food materials—1: factors affecting and industrial uses. Crit. Rev. Food Sci. Nutr. 44, 465–471. https://doi.org/10.1080/10408690490886692.

IFTPS (Institute For Thermal Processing Specialists), 2014. Guidelines for Conducting Thermal Processing Studies.

Inanoglu, S., Barbosa-Cánovas, G.V., Patel, J., Zhu, M.-J., Sablani, S.S., Liu, F., Tang, Z., Tang, J., 2021. Impact of high-pressure and microwave-assisted thermal pasteurization on inactivation of Listeria innocua and quality attributes of green beans. J. Food Eng. 288, 110162 https://doi.org/10.1016/j.jfoodeng.2020.110162.

Jain, D., Tang, J., Liu, F., Tang, Z., Pedrow, P.D., 2018. Computational evaluation of food carrier designs to improve heating uniformity in microwave assisted thermal pasteurization. Innovat. Food Sci. Emerg. Technol. 48, 274–286. https://doi.org/10.1016/j.ifset.2018.06.015.

Jain, D., Tang, J., Pedrow, P.D., Tang, Z., Sablani, S., Hong, Y.-K., 2019. Effect of changes in salt content and food thickness on electromagnetic heating of rice, mashed potatoes and peas in 915 MHz single mode microwave cavity. Food Res. Int. 119, 584–595. https://doi.org/10.1016/j.foodres.2018.10.036.

Luan, D., Tang, J., Pedrow, P.D., Liu, F., Tang, Z., 2013. Using mobile metallic temperature sensors in continuous microwave assisted sterilization (MATS) systems. J. Food Eng. 119, 552–560. https://doi.org/10.1016/j.jfoodeng.2013.06.003.

Luan, D., Tang, J., Pedrow, P.D., Liu, F., Tang, Z., 2015. Performance of mobile metallic temperature sensors in high power microwave heating systems. J. Food Eng. 149, 114–122. https://doi.org/10.1016/j.jfoodeng.2014.09.041.

Luan, D., Tang, J., Pedrow, P.D., Liu, F., Tang, Z., 2016. Analysis of electric field distribution within a microwave assisted thermal sterilization (MATS) system by computer simulation. J. Food Eng. 188, 87–97. https://doi.org/10.1016/j.jfoodeng.2016.05.009.

Montero, M.L., Sablani, S., Tang, J., Ross, C.F., 2020. Characterization of the sensory, chemical, and microbial quality of microwave-assisted, thermally pasteurized fried rice during storage. J. Food Sci. 85, 2711–2719. https://doi.org/10.1111/1750-3841.15384.

Nelson, S., 1973. Electrical properties of agricultural products - a critical review. Trans. ASAE (Am. Soc. Agric. Eng.) 16. https://doi.org/10.13031/2013.37527, 0384–0400.

Peng, J., Tang, J., Barrett, D.M., Sablani, S.S., Anderson, N., Powers, J.R., 2017. Thermal pasteurization of ready-to-eat foods and vegetables: critical factors for process design and effects on quality. Crit. Rev. Food Sci. Nutr. 57, 2970–2995. https://doi.org/10.1080/10408398.2015.1082126.

Piñeiro, G., Perelman, S., Guerschman, J.P., Paruelo, J.M., 2008. How to evaluate models: observed vs. predicted or predicted vs. observed? Ecol. Model. 216, 316–322. https://doi.org/10.1016/j.ecolmodel.2008.05.006.

Qu, Z., Tang, Z., Liu, F., Sablani, S.S., Ross, C.F., Sankaran, S., Tang, J., 2021. Quality of green beans (Phaseolus vulgaris L.) influenced by microwave and hot water pasteurization. Food Control 124, 107936. https://doi.org/10.1016/j.foodcont.2021.107936.

Resurreccion, F.P., Tang, J., Pedrow, P., Cavalieri, R., Liu, F., Tang, Z., 2013. Development of a computer simulation model for processing food in a microwave assisted thermal sterilization (MATS) system. J. Food Eng. 118, 406–416. https://doi.org/10.1016/j.jfoodeng.2013.04.021.

Ryynänen, S., 1995. The electromagnetic properties of food materials: a review of the basic principles. J. Food Eng. 26, 409–429. https://doi.org/10.1016/0260-8774(94)00063-F.

Sablani, S.S., Bruno, L., Kasapis, S., Symaladevi, R.M., 2009. Thermal transitions of rice: development of a state diagram. J. Food Eng. 90, 110–118. https://doi.org/10.1016/j.jfoodeng.2008.06.008.

Tang, J., 2015. Unlocking potentials of microwaves for food safety and quality. J. Food Sci. 80, E1776–E1793. https://doi.org/10.1111/1750-3841.12959.

Tang, J., Lelievre, J., Tung, M.A., Zeng, Y., 1994. Polymer and ion concentration effects on gellan gel strength and strain. J. Food Sci. 59, 216–220. https://doi.org/10.1111/j.1365-2621.1994.tb06934.x.

Tang, J., Tung, M.A., Lelievre, J., Zeng, Y., 1997. Stress-strain relationships for gellan gels in tension, compression and torsion. J. Food Eng. 31, 511–529. https://doi.org/10.1016/S0260-8774(96)00087-8.

Tang, J., Hong, Y.-K., Inanoglu, S., Liu, F., 2018. Microwave pasteurization for ready-to-eat meals. Curr. Opin. Food Sci. 23, 133–141. https://doi.org/10.1016/j.cofs.2018.10.004.